ACS APPLIED MATERIALS & INTERFACES

Research Article

www.acsami.org

Novel Au Catalysis Strategy for the Synthesis of Au@Pt Core−Shell Nanoelectrocatalyst with Self-Controlled Quasi-Monolayer Pt Skin

Youlin Zhang,[†,§,∥] Xiaokun Li,[†,∥] Kai Li,[‡] Bin Xue,[§] Chunmei Zhang,[†] Cheng Du,[†] Zhijian Wu,[‡] and Wei Chen[*,†]

[†]State Key Laboratory of Electroanalytical Chemistry, Changchun Institute of Applied Chemistry and [‡]State Key Laboratory of Rare Earth Resource Utilization, Changchun Institute of Applied Chemistry, Chinese Academy of Sciences, Changchun 130022, China

[§]State Key Laboratory of Luminescence and Applications, Changchun Institute of Optics, Fine Mechanics and Physics, Chinese Academy of Sciences, Changchun 130033, China

Supporting Information

ABSTRACT: Design of catalytically active Pt-based catalysts with minimizing the usage of Pt is a major issue in fuel cells. Herein, for the first time, we have developed a Au catalytic reduction strategy to synthesize a Au@Pt core−shell electrocatalyst with a quasi-monolayer Pt skin spontaneously formed from the gold surface catalysis. In the presence of presynthesized gold nanocrystals (used as the catalyst and Au seeds) and 4-(2-hydroxyethyl)-1-piperazineethanesulfonic acid buffer (used as reductant), under the Au surface catalysis, platinum ions can be reduced and deposited on the gold nanocrystals to form a Pt skin surface with a quasi-monatomic thickness. In the present strategy, Pt ions can be reduced only under the catalysis of gold surface and thus when the surface of Au NPs is covered by a monatomic Pt layer, the reduction reaction of Pt ions will be spontaneously turned off. Therefore, the significant advantage of this synthesis strategy is that the formation of quasi-monolayer Pt skin surface can be self-controlled and is completely free of controlling the dosage of platinum ions and the size distribution of Au cores. The synthesized Au@Pt core@shell structure exhibited enhanced electrocatalytic activities for oxygen reduction reaction and methanol oxidation reaction, which are 6.87 and 10.17 times greater than those of Pt/C catalyst, respectively. The present study provides a new strategy for obtaining high-performance bimetallic/multimetallic electrocatalysts with high utilization of precious metals.

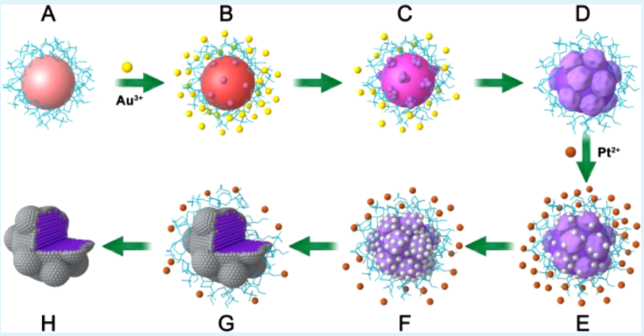

KEYWORDS: *electrocatalyst, catalytic reduction strategy, Pt skin, oxygen reduction reaction, methanol oxidation reaction*

1. INTRODUCTION

Considering the long-term trend of energy shortage in future, fuel cell technologies, such as proton-exchange membrane fuel cells, direct methanol fuel cells, and alkaline fuel cells, are believed to be the next generation of energy solutions and have attracted much attention in the past decades.[1] In these fuel cells, electrocatalysts on both anode and cathode play a key role in improving the power density and energy conversion efficiency.[2−4] Because of their unique catalytic properties, platinum (Pt)-based nanostructured materials are the most widely used electrocatalysts for the oxygen reduction at cathode and fuel oxidation at anode.[5−8] Nevertheless, Pt-based catalysts are usually poisoned by CO-like intermediates generated from the fuel oxidation, which can seriously lower Pt catalytic performances.[9] In addition, other drawbacks, including low electrochemical stability, high cost, and scarce reserve, also severely restrict the wide applications of Pt-based electrocatalysts in commercial fuel cells. Therefore, attempts on reducing Pt usage as low as possible and increasing active sites of Pt as much as possible are of critical importance in exploring novel Pt-based catalysts for fuel cells.[10−14]

On the basis of these considerations, Pt-based bimetallic/multimetallic catalysts with various morphologies, such as alloyed structures[15−19] and core−shell structures,[20−22] have been largely investigated for reducing platinum usage and improving catalytic activity. In principle, only surface Pt atoms of Pt-based nanoparticles (and possibly subsurface Pt atoms) can provide catalytically active sites, whereas internal atoms are almost not involved in the catalytic reactions.[23] Therefore, Pt-based alloy and core−shell structures have their respective advantages and shortcomings. Pt-based alloy nanostructures have enhanced electrocatalytic performances due to the strongly intermetallic interactions, but a large amount of Pt atoms inside the alloys are actually not utilized. For the core−shell nanostructures with a Pt shell, the reported Pt shells

Received: June 8, 2017
Accepted: September 8, 2017
Published: September 8, 2017

DOI: 10.1021/acsami.7b08210
ACS Appl. Mater. Interfaces 2017, 9, 32688−32697

usually have a thickness of 2−5 nm.[6] Meanwhile, although fabrication of core−shell nanostructure is an effective way to reduce platinum usage, a too thick Pt shell can not only hamper significantly the interactions between core and shell materials but also reduce the efficient utilization of Pt. Therefore, a thin Pt skin surface coated over the core materials with a monatomic layer is an ideal Pt-based electrocatalyst.[24] To this end, various synthetic methods, such as high-temperature annealing, electrochemical deposition, displacement reaction, and spontaneous deposition, have been developed to construct Pt skin with the thickness range from submonolayer to multilayers.[24−33] In all of these works, to achieve the wanted thickness of Pt layers, the dosage of Pt has to be accurately calculated and carefully controlled according to the size and surface structure of core. However, it is almost impossible to prepare core materials with completely uniform size, which makes it difficult to precisely control the thickness of Pt layers on the core.[34] In addition, the calculations and careful control of experimental condition also largely complicate the synthesis process. Therefore, preparing tailored core@shell nanostructures with an ultrathin Pt skin surface with more convenient methods is still a substantial challenge.

Recently, the use of Au surface as catalytic active sites for precious-metal deposition has become a very attractive approach, for example, underpotential deposition, which can engineer the architectural diversity of metal nanoparticles by rationally and independently arranging every framework-determining element.[35−37] Herein, for the first time, we developed a different Au catalytic reduction strategy to synthesize Pt skin electrocatalyst with a quasi-monatomic layer (about 1.3 atomic layers) at room temperature. Au nanoparticles were chosen as core materials because the Au@Pt core−shell structures have shown improved catalytic performances compared to Pt nanoparticles (NPs) partly due to the lattice mismatch at the interface of Au core and Pt shell.[38−40] To increase the specific surface area of the Au@Pt electrocatalyst, the popcorn-like Au nanocrystals (denoted as Au PNPs) were first synthesized as core, and a Pt skin surface with 1.3 atomic layers (denoted as Au@Pt PNPs) was formed under the gold surface catalysis. Particularly, two key points of this novel synthesis method should be noted. First, the quasi-monolayer Pt shell is spontaneously formed on the Au PNPs based on the catalytic properties of Au surface. When the surface of Au PNPs is fully covered by a monolayer of Pt atoms, the reduction process can be terminated even if there are free Pt ions. Therefore, the formation of Pt skin surface on Au cores with a quasi-monatomic layer can be self-controlled with no need to precisely control the amount of Pt used and the uniform size of Au nanocrystal cores. Second, the synthesis process is very facile and friendly. On the basis of the gold catalytic reduction strategy, the reaction occurs under more mild conditions (room temperature and near neutral solution) with a shorter reaction time (within 2 h) compared to the harsh conditions of other synthetic methods, such as high temperature, time consuming (even several days), complicated processes, and/or the use of strong acid and alkali solvents. Moreover, the Au@Pt PNPs exhibited enhanced catalytic activities for both oxygen reduction reaction (ORR) and methanol oxidation reaction (MOR) by comparing with the commercial Pt/C catalyst. The present catalytic reduction strategy provides a new route to synthesize core@shell nanostructured electrocatalysts with ultrathin precious-metal surface.

2. EXPERIMENTAL SECTION

2.1. Chemicals. Potassium tetrachloroplatinate(II) (K_2PtCl_4) and hydrogen tetrachloroaurate(III) trihydrate ($HAuCl_4{\cdot}3H_2O$) were obtained from Sigma-Aldrich Co. 4-(2-Hydroxyethyl)-1-piperazineethanesulfonic acid (HEPES) was purchased from Dingguo Biotechnology Co. Ltd. (Beijing, China). Other analytical chemicals were obtained from Beijing Chemical Reagents Co. Ltd. (Beijing, China) and used without further purification. Milli-Q water (18.2 MΩ cm) was used in all experiments.

2.2. Material Characterization. The size and morphology of the nanostructures were measured by field emission scanning electron microscopy (FESEM, Hitachi S-4800) and transmission electron microscopy (TEM, Hitachi H-600). High-resolution TEM images (HRTEM), high-angle annular dark-field scanning transmission electron microscopy (HAADF-STEM) images, element analysis mapping, and energy-dispersive X-ray spectroscopy (EDX) were performed on a JEM-2010 (HR) microscope operated at 200 kV. Powder X-ray diffraction patterns of the nanostructures were investigated on a Bruker D8 Avance X-ray diffractometer with a Cu Kα radiation source (λ = 1.54 Å) between 2θ degrees of 10 and 90°. The X-ray photoelectron spectroscopy (XPS) measurements for the element and structure analysis of the products were recorded on a VG Thermo ESCALAB 250 spectrometer operated at 120 W with pass energy mode at 100 eV. The compositions of the products were determined by an inductively coupled plasma mass spectrometer (Thermo Scientific Xseries II). UV−visible (UV−vis) absorption spectra were obtained on a 3101PC UV−vis−NIR scanning spectrophotometer.

2.3. Synthesis of Popcorn-Like Au Nanostructures (Au PNPs). The citrate-stabilized spherical gold nanoparticles (Au NPs) with an average diameter of 15 nm were first synthesized according to the traditional Turkevich−Frens method.[41,42] For the synthesis of Au PNPs, the citrate-stabilized Au NPs were centrifuged and then added to the HEPES buffer (pH 7.5, aqueous solution) to obtain a 10 mL mixture solution with 2.0 nM Au NPs and 10 mM HEPES. After the incubation of the mixture for 5 min, 0.2 mL of 1% $HAuCl_4$ aqueous solution was added. The color of the solution changed from reddish to blue-purple within 1 min. The popcorn-like Au nanocrystals (Au PNPs) were obtained in HEPES buffer after 10 min incubation without shaking at room temperature.

2.4. Synthesis of Popcorn-Like Au@Pt Nanocrystals with Monolayer-Like Pt Skin Surface (Au@Pt PNPs). K_2PtCl_4 solution (0.2 mL, 50 mM) was added to the preprepared Au PNP solution (containing about 2 nM Au PNPs and 10 mM HEPES buffer with pH 7.5). After 1 h incubation at room temperature, Au@Pt PNPs with monatomic-like Pt skin surface were obtained. Excess Pt^{2+} in solution were removed by repeated centrifugation (two times) and then the product was redispersed in water for characterization or in a mixture containing water and Nafion (5%) (v/v 5:0.025) to form a 1.6 mg/mL catalyst ink and stored at 4 °C.

2.5. Electrochemical Measurements. The electrochemical measurements were carried out with a CHI 750D electrochemical workstation and a conventional three-electrode cell. The catalytic activities were measured with a rotating disk electrode (RDE). A Pt wire and a Ag/AgCl electrode (in saturated KCl solution) were used as the counter and reference electrodes, respectively. High-purity nitrogen (99.99%) or oxygen (99.99%) was used for deaeration of the solutions. The used electrolyte is 0.1 M $HClO_4$ or KOH solution. Prior to each electrochemical measurement, the electrolyte solutions were saturated with nitrogen (N_2) or oxygen (O_2) and protected with the corresponding atmosphere during the experimental procedures. All electrochemical experiments were carried out at room temperature. For the ORR measurements, to prepare a catalyst-coated working electrode, 20 μL of 1.6 mg mL^{-1} catalyst ink (Au@Pt PNPs), 10 μL of 2.0 mg mL^{-1} commercial Pd/C catalyst solution (containing 0.5% Nafion), or 20 μL of 1.6 mg mL^{-1} Au PNPs (containing 0.5% Nafion) was drop-coated on the polished RDE surface (5 mm in diameter) using a micropipettor. The catalyst-coated working electrode was then evaporated at room temperature. To clean and activate the electrode surface, the working electrode was electrochemically cycled between

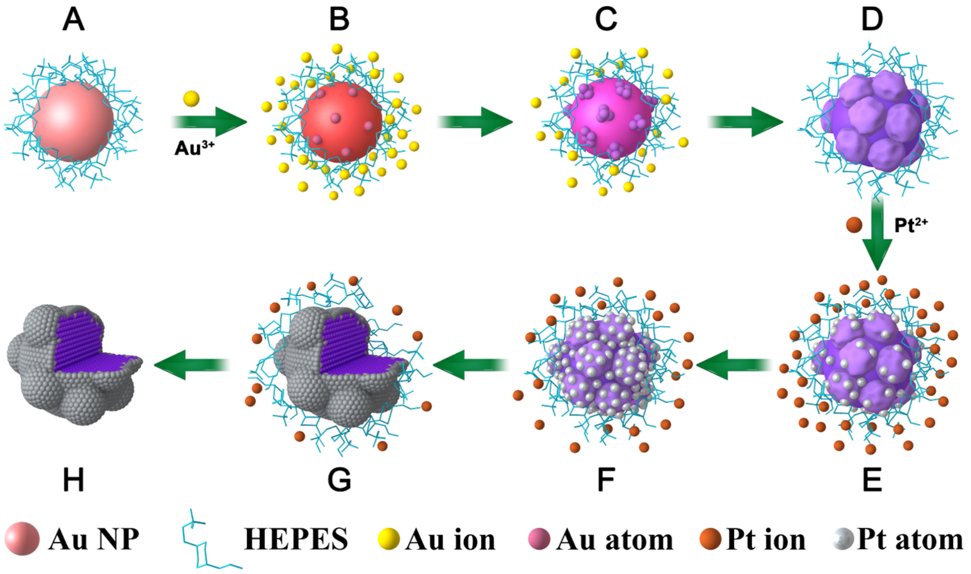

Figure 1. Schematic diagram of the two-step synthesis of Au@Pt PNPs with quasi-monolayer Pt skin surface using Au catalytic reduction strategy. (A) Mixed solution of Au NPs and HEPES; (B−D) gradual reduction of Au ions on the surface of Au NPs to form popcorn-like Au NPs (Au PNPs); (E, F) gradual reduction of Pt ions to Pt atoms on the surface of Au PNPs to form Au@Pt PNPs; (G) Au@Pt PNPs with excess free Pt ions in solution, and (H) formation of Au@Pt PNPs with monatomic-like Pt skin.

−0.2 and 1.0 V at a scan rate of 100 mV s^{-1} in 0.1 M $HClO_4$ solution (N_2-saturated) and then cycled between −0.9 and 0.2 V in 0.1 M KOH solution (N_2-saturated) until reproducible cyclic voltammograms were obtained. Cyclic voltammetric (CV) curves were recorded at a scan rate of 50 mV s^{-1} in 0.1 M KOH solution. For CO stripping measurements, the surface of catalysts was first preadsorbed by CO at −0.8 V (vs Ag/AgCl) by bubbling CO in solution and then the CO was degassed in the electrolyte by bubbling N_2. ORR polarizations were measured on a Princeton Applied Research Model (PAR) 636 Ring-Disk electrode system and obtained in a 0.1 M O_2-saturated KOH solution at rotating rates ranging from 225 to 1600 rpm with a scan rate of 10 mV s^{-1}. A durability test of the catalysts was performed by continuously potential cycling between −0.4 and 0.2 V at a scan rate of 100 mV s^{-1} in an O_2-saturated 0.1 M KOH solution. For the MOR measurements, the electrocatalytic activity of working electrode coated with Au@Pt PNPs or the commercial Pt/C catalyst or Au PNPs was evaluated in 0.1 M KOH solution containing 0.5 M methanol by recording the CVs from −0.9 to 0.65 V for Au@Pt PNPs or from −0.9 to 0.2 V for commercial Pd/C catalyst and Au PNPs. The chronoamperometric curves were measured at 0.2 V for 800 s.

2.6. Density Functional Theory (DFT) Calculations. The theoretical calculations were carried out with the Vienna ab-initio simulation package (VASP).[43,44] Here, Blöchl's all-electron-like projector augmented wave (PAW) method was used to deal with the interactions between ion cores and valence electrons.[45,46] Perdew−Burke−Ernzerhof (GGA-PBE) exchange-correlation functional was used.[47] A Fermi scheme with an energy smearing of 0.1 eV was used to determine the electron occupancies. Meanwhile, the Monkhorst−Pack method was used for the Brillouin zone integration.[48] The optimization of geometries was performed with energy and force converged to 1.0×10^{-6} eV atom^{-1} and 0.01 eV Å^{-1}, respectively. Due to the presence of magnetic atom, spin polarization was considered in the calculations. The surface of Au@Pt(111) is obtained by cutting Au bulk (fcc) along the [111] direction. A four-layer slab was selected as the thickness of surface slab. The Au@Pt with Pt monolayer is obtained by modifying the pure Au(111) by replacement of one surface Au with Pt atoms, and the Au@Pt slabs are relaxed to gain the stable slab structures. Because the detail consistent of Au@Pt(111) cannot be observed in the experiment, six configurations (Table S1) are considered in our calculations. In structural optimization calculations, the atom positions in the bottom layer were fixed and the three top surface layers were relaxed. To avoid the periodic interactions, a vacuum layer of 12 Å was used along the *c* direction normal to the surface. The coverage of a 1/9 monolayer was treated with a (3 × 3) supercell. The chemisorption energies of oxygen on Au@Pt(111) surfaces, ΔE_{ads}, is defined as follows

$$\Delta E_{\text{ads}} = E_{\text{adsorbate/slab}} - (E_{\text{slab}} + E_{\text{adsorbates}})$$

where $E_{\text{adsorbate/slab}}$ refers to the total energy of adsorbate on the Au@Pt surface, E_{slab} represents the energy of the Au@Pt surface, and $E_{\text{adsorbate}}$ represents the energy of single O atom. Same parameters were used for the calculation of the first two terms, and the calculation of the third term was realized by supposing that the isolated adsorbate is in a box of 12 × 12 × 12 Å^3. The negative ΔE_{ads} indicates exothermic chemisorption.

3. RESULTS AND DISCUSSION

3.1. Synthesis Mechanism. The Au@Pt core@shell nanocrystal with a quasi-monolayer Pt skin (Au@Pt PNPs) was obtained by a two-step synthesis process, as shown in Figure 1. In the first step (Figure 1A−D), to increase the catalytic surface area of electrocatalyst, the popcorn-like Au nanoparticles (Au PNPs) were synthesized from a three-component solution containing Au^{3+} ions (to form the popcorn-like structures), HEPES (used as the reductant), and 15 nm spherical gold nanoparticles (Au NPs, used as the catalyst and seeds). Here, the Au^{3+} ions added into the mixed solution of Au NPs and HEPES (Figure 1A) were reduced to Au atoms by HEPES under the catalysis of Au NP surface. Due to the self-catalytic effect, Au atoms were deposited on some specific facets of the Au NPs (Figure 1B) to form small popcorn-like islands (Figure 1C). The Au PNPs were eventually synthesized accompanying with total consumption of Au^{3+} ions in the solution (Figure 1D). In the next step (Figure 1E−H), the Au PNPs were used as both Au core and the catalyst for the formation of Au@Pt core@shell structure with Pt skin surface. After adding enough Pt ions into the above mixed solution (HEPES and Au PNPs), the Pt ions were reduced to Pt atoms by HEPES under the catalysis of Au PNPs. On the basis of the calculations and theoretical studies below, the Pt skin has a thickness of about 1.3 atomic layers. We

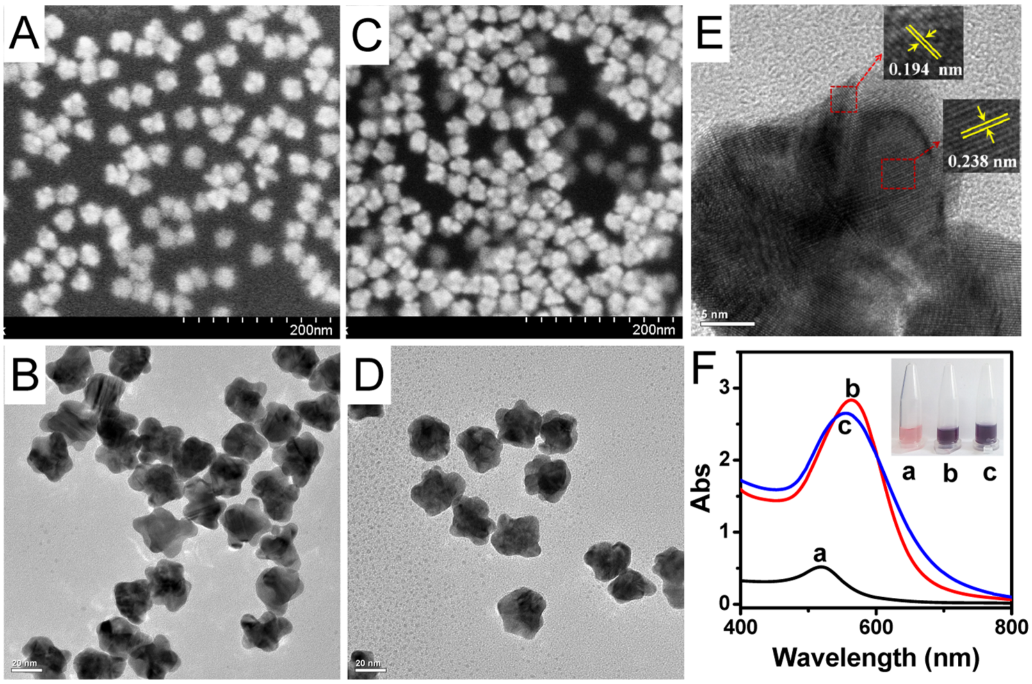

Figure 2. Scanning electron microscopy (SEM) (A) and TEM (B) images of Au PNPs. SEM (C) and TEM (D) images of Au@Pt PNPs. (E) High-resolution TEM image of Au@Pt PNPs. (F) UV−vis absorption spectra of (a) Au NPs, (b) Au PNPs, and (c) Au@Pt PNPs in aqueous solution and their corresponding photographs.

proposed that Pt atoms were first deposited randomly on the surface of the Au PNPs to form an Au_3Pt_1 alloy monolayer, that is, there is an approximately 0.3 atomic layer of Pt on Au surface (Figure 1E). Then, one more layer of Pt atoms was deposited on the Au_3Pt_1 surface to form a Au@Pt core@shell structure with a total of 1.3 layers of Pt skin (from Figure 1F,G). When the surface of Au PNPs was fully covered with Pt monolayer, without the catalysis of exposed Au surface, HEPES could not continue to reduce Pt ions to Pt atoms although there are excess free Pt ions in solution (Figure 1G). As a result, Au@Pt PNPs with monatomic-like Pt skin can be obtained (Figure 1H).

The formation of Au islands and Pt skin under the same catalytic reduction conditions could probably be attributed to the different Au catalytic mechanisms. For Au ions, there is a high reduction rate mediated by an autocatalytic process.[49] In previous reports, HEPES could reduce Au ions to form branched or nanoflower-like gold nanocrystals in the absence of Au NPs.[50,51] In our system, the reduced Au atoms tend to nucleate on the surface of Au NPs rather than in solution alone. The Au nuclei can serve as catalytic sites for further reduction of Au ions. Therefore, Au islands rather than films were formed on the surface of Au NP seeds. By contrast, unlike the autocatalytic process of Au, the reduced Pt atoms were evenly deposited on the surface of Au PNPs under the Au catalytic reduction condition. Therefore, monolayer-like Pt skin surface can be obtained.

It should be pointed out that the exact mechanism is not clear that 1.3 rather than 1 atomic layer of Pt skin surface can be formed by this Au catalytic reduction strategy. We speculate that the first 0.3 atomic layer of Pt is assimilated by Au surface atoms and then these Pt atoms show similar catalytic behavior to Au substrate, which leads to the formation of another monolayer of Pt atoms covered on the formed Au_3Pt_1 surface. Eventually, the catalytic reduction synthesis process was terminated by the formation of Pt skin surface with quasi-monoatomic layer on Au core.

3.2. Characterization. The morphologies of the obtained nanostructures were characterized by TEM and FESEM. The initial 15 nm Au NPs appear to be spherical and nearly monodisperse (Figure S1). By contrast, as shown in Figure 2A,B, the synthesized Au PNPs show popcorn-like morphology with irregular convex surface with average diameter of 28.52 ± 0.80 nm. After the formation of Pt skin on the Au PNPs, the Au@Pt PNPs present no obvious change of morphology and size compared to the Au PNPs (Figure 2C,D). To further explore the crystal structure of the Au@Pt PNPs, an HRTEM image is shown in Figure 2E. Careful measurements indicated that there are mainly two types of lattice fringes with interplanar spacing of 2.38 and 1.94 Å, corresponding to the (111) and (200) crystal planes of Au particles, respectively. The UV−vis absorption spectra of spherical Au NPs, Au PNPs, and Au@Pt PNPs in aqueous solution and their photographs are shown in Figure 2F. Different from the characteristic red appearance of Au NPs with an absorption peak at 519 nm, the colloidal solutions of Au PNPs and Au@Pt PNPs are blue-purple with absorption peaks at 564 and 557 nm, respectively. The significant red shift of the absorption peak of Au PNPs or Au@Pt PNPs can be understood qualitatively by the plasmon hybridization theory, which has also been found from gold nanoflowers.[51] We note that after coating a quasi-monolayer Pt skin surface, the absorption peak of Au@Pt PNPs presents a slight blue shift compared with the Au PNPs, which attributes to the near-UV absorption of small Pt nanoparticles (<50 nm) in aqueous solution.[52] In addition, to check if the Au@Pt PNPs with monolayer-like Pt skin surface can continue to catalyze HEPES to reduce Pt^{2+}, the UV−vis spectra of the mixture solutions containing Au@Pt PNPs and additional Pt^{2+} were recorded, as shown in Figure S2. No obvious change can be observed for the spectra of Au@Pt PNPs before and after

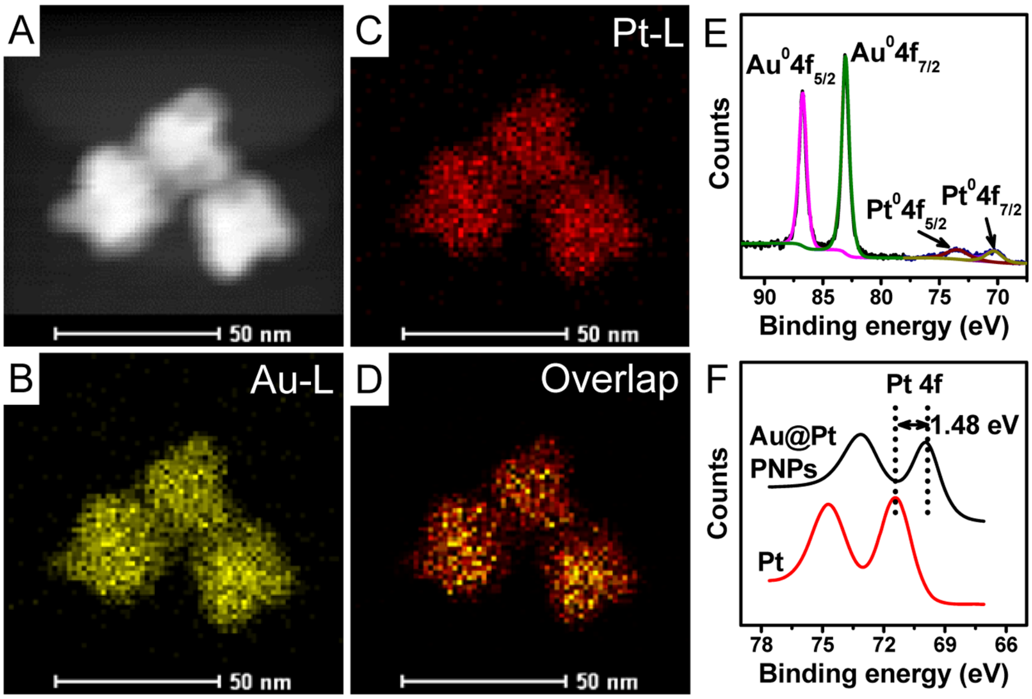

Figure 3. (A) HAADF-STEM image of Au@Pt PNPs. Elemental mapping images of Au (B), Pt (C), and their overlap (D). High-resolution XPS images of Au 4f (E) and Pt 4f (F).

adding Pt^{2+} in the solution, which indicates that HEPES cannot reduce Pt ions when Au surface is fully covered with Pt layer. As a mild reducing agent, HEPES can reduce gold ions to form gold nanoparticles, but cannot reduce platinum ions, which may be due to the much lower standard electrode potential of $PtCl_4^{2-}$ (0.758 V vs NHE) compared to Au^{3+} (1.36 V vs NHE). Above results show that the catalytic reduction process for Pt^{2+} deposition can only occur in the presence of Au substrates, and Au surface catalysis is a basic requirement for the reduction of Pt ions by HEPES. The exact mechanism will be investigated in our subsequent work.

The EDX analysis shown in Figure S3 indicates the presence of Au and Pt in the Au@Pt PNPs. The distribution of Au and Pt in the Au@Pt PNPs was further analyzed by HAADF-STEM. As shown in Figure 3A–D, Au is mainly distributed in the core of nanocrystals and Pt is coated on the surface of core with a very low thickness. Figure S4 displays the diffraction rings of the selected area electron diffraction (SAED) pattern, showing the polycrystalline nature of the Au@Pt PNPs. X-ray diffraction spectra were measured to further study the change of crystal structure of the nanostructures, as shown in Figure S5. Both materials present very strong and similar diffraction peaks, which agree well with the standard diffraction data of Au face-centered cubic (fcc) crystal structure (blue bar, JCPDS 65-2870). However, there is no diffraction signal from Pt fcc crystal structure (magenta bar, JCPDS 65-2868), which could be attributed to the thin Pt shell in the Au@Pt PNPs. Such phenomenon has also been observed in other nanostructured materials with a monatomic Pt layer.[23] The chemical states and contents of Au@Pt PNPs were determined by XPS measurements. Figure 3E shows the deconvoluted XPS spectra of Au 4f and Pt 4f. The peaks at 69.96 and 73.13 eV in the Pt 4f spectrum are from the binding energies of Pt^0 $4f_{7/2}$ and Pt^0 $4f_{5/2}$, respectively. These binding energies confirm the zero-valent state of Pt in the Au@Pt PNPs. Meanwhile, it can be seen from Figure 3F that compared to the Pt/C catalyst, the binding energy presents a large negative shift (1.48 eV), which indicates that there is a partial charge transfer from Au core to the monolayer-like Pt skin. Such electron transfer could lower the binding energy of Pt—O and result in the enhanced ORR activity of the Au@Pt PNPs. In addition, the Au@Pt PNPs also showed different bulk and surface Pt/Au ratios (3.23% vs 7.00%, as determined by inductively coupled plasma-mass spectrometry (ICP-MS) and XPS, respectively), suggesting a Pt skin surface screening a Au-rich core.[24]

In addition, to probe the morphology of Pt atoms assembled on the Au NP surface, in the presence of spherical Au NPs (31 nm in diameter, which is close to that of the Au PNPs) and HEPES buffer (10 mM, pH 7.5), enough Pt^{2+} ions were added to obtain Au@Pt NPs with Pt skin (Pt/Au% ratio is 3.82%, as determined by ICP-MS). TEM images of the Au NPs and Au@Pt NPs are shown in Figure S6. Both samples show similar spherical structures, suggesting that Pt can be deposited on the surface of Au NPs without changing the morphology of Au NPs.

The thickness of Pt skin in the Au@Pt PNPs was first evaluated on the basis of the Pt content (determined by ICP-MS) and the size of Au core. Here, due to the irregular morphology of popcorn-like Au@Pt PNPs, the spherical Au@Pt NPs (shown in Figure S6B) were used to calculate the thickness of Pt shell (see Supporting Information for details). The calculated results show that there are about 1.23 atomic layers of Pt formed on the Au core. In addition, CO stripping method was used to assess the Pt skin thickness of the Au@Pt PNPs. The electrochemical surface area (ESA) of Au@Pt PNPs was measured by integrating the CO oxidation charge based on 420 $\mu C\ cm^{-2}$.[29] The CO stripping curves of Au@Pt PNPs and the commercial Pt/C catalyst are shown in Figures S7 and S8, respectively. The ESA of Au@Pt PNPs was calculated to be 187 $cm^2\ g^{-1}$. On the basis of the theoretical ESA of Pt (237 $cm^2\ g^{-1}$),[53] the Pt atoms on the surface of the Au@Pt PNPs are estimated to be about 79% of the total Pt atoms, which are

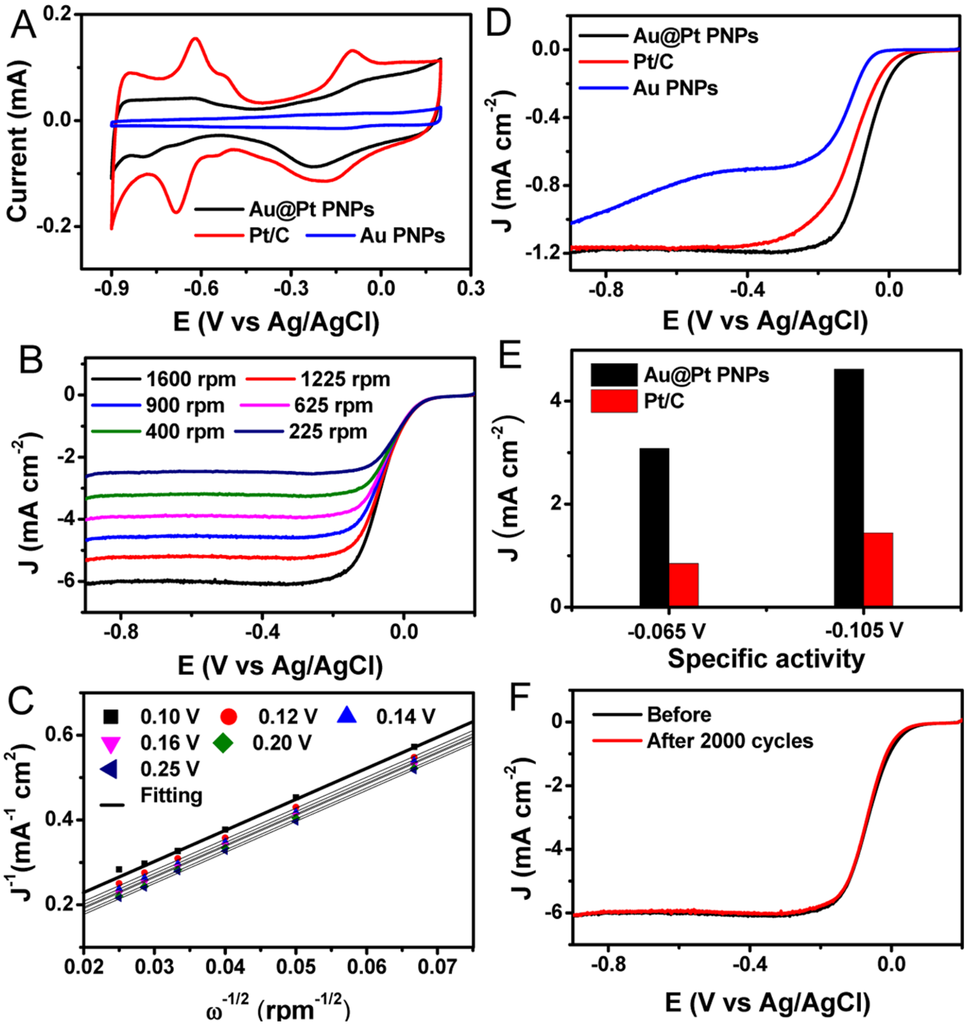

Figure 4. (A) CVs of the Au@Pt PNPs, commercial Pt/C, and Au PNPs in N_2-saturated 0.1 M KOH solution. (B) ORR polarization curves of the Au@Pt PNPs in O_2-saturated 0.1 M KOH solution at a scan rate of 10 mV s^{-1} over a range of rotation rates from 225 to 1600 rpm. (C) Koutecky−Levich plots (J^{-1} vs $\omega^{-1/2}$) from Au@Pt PNPs at different potentials. (D) ORR polarization curves of Au@Pt PNPs, commercial Pt/C, and Au PNPs in O_2-saturated 0.1 M KOH solution at 1600 rpm. (E) Specific kinetic current densities of ORR on Au@Pt PNPs and commercial Pt/C at −0.065 and −0.105 V (vs Ag/AgCl), respectively. (F) Polarization curves of the Au@Pt PNPs before and after 2000 potential cycles in O_2-saturated 0.1 M KOH solution.

consistent with the above calculated result. Therefore, the thickness of the Pt skin surface on Au@Pt PNPs should be about 1.3 atomic layers, as schematically presented in Figure 1.

3.3. Electrocatalytic Activity of Au@Pt PNPs for Oxygen Reduction Reaction (ORR). The electrocatalytic activities of the Au@Pt PNPs for ORR were then studied by voltammetric measurements. For comparison, the commercial Pt/C catalyst (20% by weight of Pt on Vulcan XC-72 carbon support) and the Au PNPs were also examined. Figure 4A shows the CVs of the three samples in N_2-saturated 0.1 M KOH solution at a sweep rate of 50 mV s^{-1}. It can be seen that the Au PNPs show a featureless CV in the studied potential range. However, after the formation of Pt skin on the Au PNPs, the voltammetric features of Pt can be seen clearly, including the hydrogen adsorption/desorption in the range of −0.83 to −0.45 V and the oxidation of Pt/reduction of Pt oxides in the range of −0.20 to 0.08 V (black curve in Figure 4A). Due to the thin Pt skin, the current of hydrogen adsorption/desorption from Au@Pt PNPs is smaller than that from the Pt/C catalyst (red curve). Furthermore, the electrochemical behaviors of the prepared samples were studied within a wider potential window from −0.9 to 0.65 V. As shown in Figure S9, for the Au PNPs, there is a large reduction current peak at 0.13 V from the Au oxide reduction. However, for the Au@Pt PNPs, the reduction current peak from the Au oxide reduction cannot be observed. Such result suggests that a fully Pt atomic layer has been formed on the surface of Au particle core with the present synthesis strategy.

To further study the catalytic properties of Au@Pt PNPs, a series of ORR polarization curves were recorded in oxygen-saturated KOH solution at a scan rate of 10 mV s^{-1} and rotation rates ranging from 225 to 1600 rpm (Figure 4B). On the basis of the slopes of the Koutecky−Levich plots obtained from Au@Pt PNPs (Figure 4C), the number of electrons involved per oxygen reduction is 4.1 (detailed calculations are included in the Supporting Information), which indicates that O_2 is directly reduced to H_2O mainly by a four-electron pathway.[16] Figure 4D compares the ORR polarization curves of the studied three samples at the rotation speed of 1600 rpm. Clearly, both the onset potential and half-wave potential of ORR on Au@Pt PNPs are more positive than those on commercial Pt/C and Au PNPs. For instance, the half-wave

DOI: 10.1021/acsami.7b08210
ACS Appl. Mater. Interfaces 2017, 9, 32688−32697

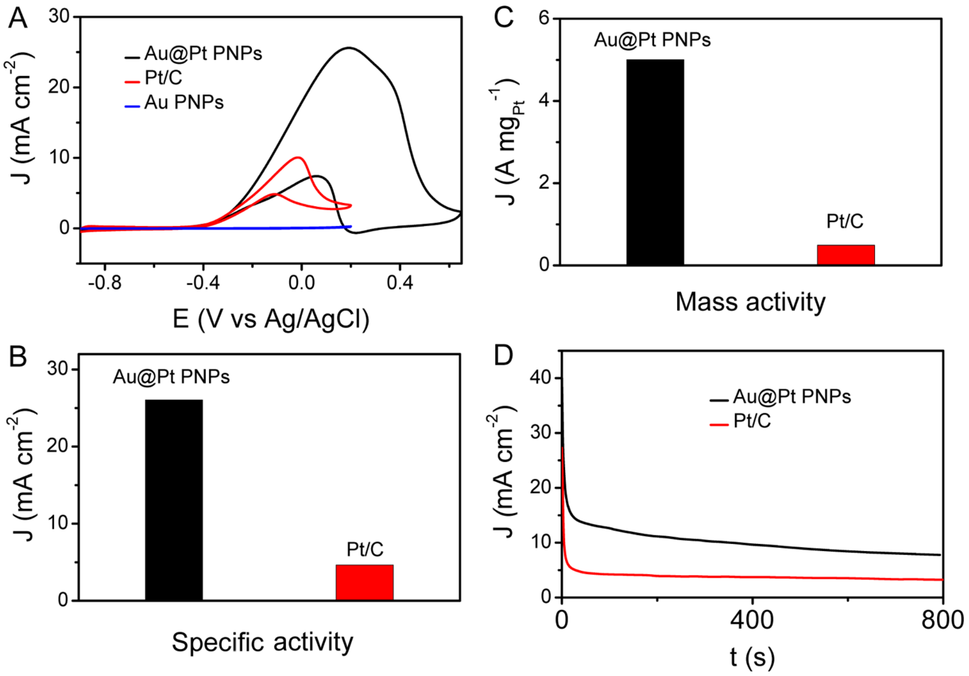

Figure 5. (A) CV curves in 0.1 M KOH solution containing 0.5 M methanol. Specific activities (B) and mass activities (C) of Au@Pt PNPs at 0.2 V and Pt/C catalyst at 0 V. (D) Stability tests at 0.2 V for Au@Pt PNPs and at 0 V for Pt/C catalyst.

potentials on the Au@Pt PNPs, commercial Pt/C, and Au PNPs are −0.065, −0.105, and −0.117 V, respectively. On the basis of the electrochemical results, the corresponding specific activities of Au@Pt PNPs and Pt/C at −0.065 and −0.105 V (vs Ag/AgCl) were calculated and are shown in Figure 4E. Notably, the obtained specific activities from Au@Pt PNPs are 2.90 mA cm^{-2} at −0.065 V and 4.39 mA cm^{-2} at −0.105 V, which are 3.61 and 3.21 times higher than those of the commercial Pt/C catalyst (0.80 mA cm^{-2} at −0.065 V and 1.36 mA cm^{-2} at −0.105 V), respectively. Meanwhile, as shown in Figure S10, the mass activities of Au@Pt PNPs at −0.065 and −0.105 V were calculated to be 588.3 and 8.92 mA mg$_{pt}^{-1}$, which are 6.87 and 6.11 times larger than those of the commercial Pt/C catalyst (85.6 mA mg$_{pt}^{-1}$ at −0.065 V and 146 mA mg$_{pt}^{-1}$ at −0.105 V), respectively. In addition, accelerated durability tests (ADTs) were carried out by cycling the potential between −0.4 and 0.2 V (vs Ag/AgCl) in O_2-saturated 0.1 M KOH solution at a scan rate of 100 mV s^{-1}. Figure 4F shows the polarization curves of ORR on the Au@Pt PNPs before and after 2000 potential cycles. One can see that there is no obvious change of current and half-wave potential after the ADT, suggesting the high electrochemical stability of Au@Pt PNPs for ORR. As comparison, the ORR polarization curves on the commercial Pt/C and Au PNPs show obvious negative shift after the ADTs (Figure S11), indicating the much lower catalytic durability of these two catalysts compared to that of Au@Pt PNPs. These results clearly demonstrate that the Au@Pt core@shell structure with only 1.3 atomic layers of Pt skin has excellent electrocatalytic property for ORR with enhanced activity and stability.

In addition, the electrocatalytic activities of Au@Pt core@shell structures prepared from Pt NPs (Au@Pt NPs) and Au PNPs (Au@Pt PNPs) were investigated. The ORR polarization curves of the popcorn-like Au@Pt PNPs and spherical Au@Pt NPs at the rotation speed of 1600 rpm are shown in Figure S12. Because of the rough surface of Au@Pt PNPs, the onset potential and half-wave potential of ORR on Au@Pt PNPs are more positive than those on the Au@Pt NPs. However, the half-wave potentials of both above core@shell materials are more positive than those of the commercial Pt/C catalyst. Such results indicate that the Au@Pt core@shell structure can be prepared from Au nanocrystals with different morphologies through the Au catalytic reduction strategy.

3.4. Electrocatalytic Activity of Au@Pt PNPs for Methanol Oxidation Reaction (MOR).

In addition to the ORR, methanol oxidation reaction (MOR) catalyzed by the Au@Pt PNPs was also studied. Figure 5A shows the CVs of Au@Pt PNPs, commercial Pt/C, and Au PNPs in 0.1 M KOH solution containing 0.5 M methanol at a scan rate of 50 mV s^{-1}. As usual, the Au PNPs show very low electrocatalytic activity for MOR (blue curve). Surprisingly, Au@Pt PNPs with Pt skin (black curve) shows much larger oxidation current density than the commercial Pt/C catalyst (red curve). Meanwhile, the corresponding specific activities and mass activities of Au@Pt PNPs, and commercial Pt/C for methanol oxidation were compared. As shown in Figure 5B, in the positive sweep, the maximum peak current density on Au@Pt PNPs (26.05 mA cm^{-2}) is 5.61 times higher than that on the commercial Pt/C catalyst (4.64 mA cm^{-2}). On the basis of the total amount of precious metals, for example, (Au + Pt) for Au@Pt PNPs and Pt for the commercial Pt/C catalyst, the mass activity of Au@Pt PNPs is lower than that of the commercial Pt/C catalyst (Figure S13). However, on the basis of the Pt loading, the maximum peak current density (5004 mA mg$_{Pt}^{-1}$) on Au@Pt PNPs is 10.17 times higher than that on the commercial Pt/C catalyst (492 mA mg$_{Pt}^{-1}$) (Figure 5C). To further study the activity and long-term stability of the Au@Pt PNPs and the commercial Pt/C catalyst (as a comparison) for MOR, chronoamperometric curves were recorded (Figures 5D and S14). On both samples, the initial current density drops quickly owing to the adsorption of CO-like intermediates on the catalyst surface; however, the oxidation current density from

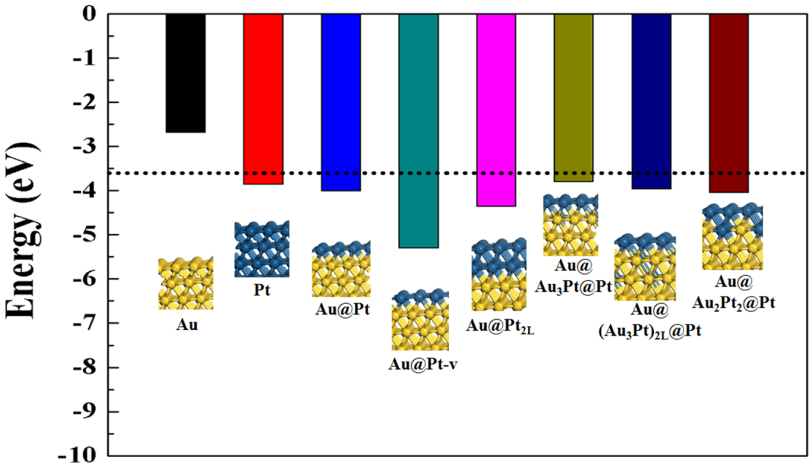

Figure 6. Oxygen adsorption energy (ΔE_{ads}) calculated with DFT for Au@Pt(111) with various layers of Pt skin. Results for Pt(111) and Au(111) are presented for comparison.

the Au@Pt PNPs has a slower decrease and the current density on Au@Pt PNPs is much higher than that on the commercial Pt/C catalyst in the whole test time of 800 s. These results indicate that the Au@Pt PNPs also have excellent electrocatalytic performance for MOR.

3.5. Density Functional Theory (DFT) Calculations. The catalytic activity of Pt for the ORR is related to the oxygen adsorption energy (ΔE_{ads}), and it was found that catalyst with a ΔE_{ads} of approximately −3.60 eV has the best ORR activity.[29] Here, we have calculated theoretically the ΔE_{ads} of various surface structures with different Pt layers on Au substrates by DFT, including the surface Pt vacancy (Au@Pt-v), one Pt monolayer (Au@Pt$_{1L}$), two Pt monolayers (Au@Pt$_{2L}$), one or two Au_3Pt_1 alloy monolayer under one Pt monolayer (Au@Au$_3$Pt$_1$@Pt or Au @(Au$_3$Pt$_1$)$_{2L}$@Pt), and one Au_2Pt_2 alloy monolayer under one Pt monolayer (Au@ Au$_2$Pt$_2$@Pt). As shown in Figure 6 and Table S1, the ΔE_{ads} (−3.80 eV) obtained from the Au substrate covered by 1.25 layers of Pt atoms, that is, the structure of Au@Au$_3$Pt$_1$@Pt, is closer to the ideal one (−3.60 V) than other configurations and even pure Pt (−3.86 eV). Such theoretical calculations agree well with the above experimental results that the Au−Pt alloy submonolayer between Au core and Pt monolayer surface can enhance the electrocatalytic activity of Au@Pt PNPs.

4. CONCLUSIONS

In summary, for the first time, we have developed a catalytic reduction strategy on Au surface for synthesizing Au@Pt core−shell nanostructure with only a quasi-monatomic layer of Pt skin at room temperature. In the present study, by using the presynthesized popcorn-like Au nanocrystals (Au PNPs) as metal cores, a monolayer-like Pt skin surface can be formed on the surface of Au PNPs under the gold surface catalysis. It should be noted that in this preparation system the Pt ions can be only reduced with the aid of gold surface. Therefore, monolayer-like Pt skin surface can be achieved easily and controlled automatically on gold cores with no need to consider the amount of Pt precursor for monolayer Pt skin and the size distribution and shape of gold cores. Moreover, although only monolayer-like Pt skin was formed, both electrochemical studies and theoretical calculations showed that the obtained Au@Pt PNPs have much higher electrocatalytic performances than commercial Pt/C for both ORR and MOR in alkaline solution. The present synthesis concept may be extended to design other high-performance bimetallic/multimetallic electrocatalysts for fuel cells with high utilization of precious metals.

■ ASSOCIATED CONTENT

Ⓢ Supporting Information

The Supporting Information is available free of charge on the ACS Publications website at DOI: 10.1021/acsami.7b08210.

More structural characterizations and electrochemical measurements (PDF)

■ AUTHOR INFORMATION

Corresponding Author

*E-mail: weichen@ciac.ac.cn.

ORCID

Wei Chen: 0000-0001-5700-0114

Author Contributions

‖Y.Z. and X.L. equally contributed to this work.

Notes

The authors declare no competing financial interest.

■ ACKNOWLEDGMENTS

This work was supported by the National Natural Science Foundation of China (Nos. 21405149, 21633008, 21575134, and 11374297) and National Key Research and Development Plan (No. 2016YFA0203200). The authors also thank associate Professor Yunchun Zhou for assistance in the HRTEM analysis.

■ REFERENCES

(1) Wang, C.; van der Vliet, D.; More, K. L.; Zaluzec, N. J.; Peng, S.; Sun, S.; Daimon, H.; Wang, G.; Greeley, J.; Pearson, J.; Paulikas, A. P.; Karapetrov, G.; Strmcnik, D.; Markovic, N. M.; Stamenkovic, V. R. Multimetallic Au/FePt$_3$ Nanoparticles as Highly Durable Electrocatalyst. *Nano Lett.* **2011**, *11*, 919−926.

(2) Mazumder, V.; Lee, Y.; Sun, S. Recent Development of Active Nanoparticle Catalysts for Fuel Cell Reactions. *Adv. Funct. Mater.* **2010**, *20*, 1224−1231.

(3) Liu, M.; Zhang, R.; Chen, W. Graphene-Supported Nanoelectrocatalysts for Fuel Cells: Synthesis, Properties, and Applications. *Chem. Rev.* **2014**, *114*, 5117−5160.

(4) Kakati, N.; Maiti, J.; Lee, S. H.; Jee, S. H.; Viswanathan, B.; Yoon, Y. S. Anode Catalysts for Direct Methanol Fuel Cells in Acidic Media:

Do We Have Any Alternative for Pt or Pt−Ru? *Chem. Rev.* **2014**, *114*, 12397−12429.

(5) Steele, B. C. H.; Heinzel, A. Materials for Fuel-Cell Technologies. *Nature* **2001**, *414*, 345−352.

(6) Yang, H. Platinum-Based Electrocatalysts with Core-Shell Nanostructures. *Angew. Chem., Int. Ed.* **2011**, *50*, 2674−2676.

(7) Chen, A.; Holt-Hindle, P. Platinum-Based Nanostructured Materials: Synthesis, Properties, and Applications. *Chem. Rev.* **2010**, *110*, 3767−3804.

(8) Qu, J.; Ye, F.; Chen, D.; Feng, Y.; Yao, Q.; Liu, H.; Xie, J.; Yang, J. Platinum-Based Heterogeneous Nanomaterials via Wet-Chemistry Approaches Toward Electrocatalytic Applications. *Adv. Colloid Interface Sci.* **2016**, *230*, 29−53.

(9) Yu, W.; Porosoff, M. D.; Chen, J. G. Review of Pt-Based Bimetallic Catalysis: From Model Surfaces to Supported Catalysts. *Chem. Rev.* **2012**, *112*, 5780−5817.

(10) Tian, N.; Zhou, Z.-Y.; Sun, S.-G.; Ding, Y.; Wang, Z. L. Synthesis of Tetrahexahedral Platinum Nanocrystals with High-Index Facets and High Electro-Oxidation Activity. *Science* **2007**, *316*, 732−735.

(11) Mahmoud, M. A.; Tabor, C. E.; El-Sayed, M. A.; Ding, Y.; Wang, Z. L. A New Catalytically Active Colloidal Platinum Nanocatalyst: The Multiarmed Nanostar Single Crystal. *J. Am. Chem. Soc.* **2008**, *130*, 4590−4591.

(12) Chen, J.; Herricks, T.; Xia, Y. N. Polyol Synthesis of Platinum Nanostructures: Control of Morphology through the Manipulation of Reduction Kinetics. *Angew. Chem., Int. Ed.* **2005**, *44*, 2589−2592.

(13) Lim, B.; Lu, X.; Jiang, M.; Camargo, P. H. C.; Cho, E. C.; Lee, E. P.; Xia, Y. N. Facile Synthesis of Highly Faceted Multioctahedral Pt Nanocrystals through Controlled Overgrowth. *Nano Lett.* **2008**, *8*, 4043−4047.

(14) Teng, X.; Liang, X.; Maksimuk, S.; Yang, H. Synthesis of Porous Platinum Nanoparticles. *Small* **2006**, *2*, 249−253.

(15) Guo, S.; Zhang, S.; Sun, X.; Sun, S. Synthesis of Ultrathin FePtPd Nanowires and Their Use as Catalysts for Methanol Oxidation Reaction. *J. Am. Chem. Soc.* **2011**, *133*, 15354−15357.

(16) He, L.-L.; Zheng, J.-N.; Song, P.; Zhong, S.-X.; Wang, A.-J.; Chen, Z.; Feng, J.-J. Facile Synthesis of Platinum−gold Alloyed String-Bead Nanochain Networks with the Assistance of Allantoin and Their Enhanced Electrocatalytic Performance for Oxygen Reduction and Methanol Oxidation Reactions. *J. Power Sources* **2015**, *276*, 357−364.

(17) Lu, Y.; Jiang, Y.; Chen, W. PtPd Porous Nanorods with Enhanced Electrocatalytic Activity and Durability for Oxygen Reduction Reaction. *Nano Energy* **2013**, *2*, 836−844.

(18) Mourdikoudis, S.; Chirea, M.; Zanaga, D.; Altantzis, T.; Mitrakas, M.; Bals, S.; Liz-Marzán, L. M.; Pérez-Juste, J.; Pastoriza-Santos, I. Governing the Morphology of Pt-Au Heteronanocrystals with Improved Electrocatalytic Performance. *Nanoscale* **2015**, *7*, 8739−8747.

(19) Zhu, Z.; Zhai, Y.; Dong, S. Facial Synthesis of PtM (M = Fe, Co, Cu, Ni) Bimetallic Alloy Nanosponges and Their Enhanced Catalysis for Oxygen Reduction Reaction. *ACS Appl. Mater. Interfaces* **2014**, *6*, 16721−16726.

(20) Sun, X.; Li, D.; Ding, Y.; Zhu, W.; Guo, S.; Wang, Z. L.; Sun, S. Core/Shell Au/CuPt Nanoparticles and Their Dual Electrocatalysis for Both Reduction and Oxidation Reactions. *J. Am. Chem. Soc.* **2014**, *136*, 5745−5749.

(21) Guo, S.; Zhang, S.; Su, D.; Sun, S. Seed-Mediated Synthesis of Core/Shell FePtM/FePt (M = Pd, Au) Nanowires and Their Electrocatalysis for Oxygen Reduction Reaction. *J. Am. Chem. Soc.* **2013**, *135*, 13879−13884.

(22) Mazumder, V.; Chi, M.; More, K. L.; Sun, S. Core/Shell Pd/FePt Nanoparticles as an Active and Durable Catalyst for the Oxygen Reduction Reaction. *J. Am. Chem. Soc.* **2010**, *132*, 7848−7849.

(23) Liu, M.; Lu, Y.; Chen, W. PdAg Nanorings Supported on Graphene Nanosheets: Highly Methanol-Tolerant Cathode Electrocatalyst for Alkaline Fuel Cells. *Adv. Funct. Mater.* **2013**, *23*, 1289−1296.

(24) Hunt, S. T.; Milina, M.; Alba-Rubio, A. C.; Hendon, C. H.; Dumesic, J. A.; Román-Leshkov, Y. Self-Assembly of Noble Metal monolayers on Transition Metal Carbide Nanoparticle Catalysts. *Science* **2016**, *352*, 974−978.

(25) Wang, C.; Chi, M.; Li, D.; Strmcnik, D.; van der Vliet, D.; Wang, G.; Komanicky, V.; Chang, K.-C.; Paulikas, A. P.; Tripkovic, D.; Pearson, J.; More, K. L.; Markovic, N. M.; Stamenkovic, V. R. Design and Synthesis of Bimetallic Electrocatalyst with Multilayered Pt-Skin Surfaces. *J. Am. Chem. Soc.* **2011**, *133*, 14396−14403.

(26) Wang, Q.; Chen, S.; Shi, F.; Chen, K.; Nie, Y.; Wang, Y.; Wu, R.; Li, J.; Zhang, Y.; Ding, W.; Li, Y.; Li, L.; Wei, Z. Structural Evolution of Solid Pt Nanoparticles to a Hollow PtFe Alloy with a Pt-Skin Surface via Space-Confined Pyrolysis and the Nanoscale Kirkendall Effect. *Adv. Mater.* **2016**, *28*, 10673−10678.

(27) Shi, G.; Yano, H.; Tryk, D. A.; Iiyama, A.; Uchida, H. Highly Active, CO-Tolerant, and Robust Hydrogen Anode Catalysts: Pt-M (M = Fe, Co, Ni) Alloys with Stabilized Pt-Skin Layers. *ACS Catal.* **2017**, *7*, 267−274.

(28) Kang, Y.; Snyder, J.; Chi, M.; Li, D.; More, K. L.; Markovic, N. M.; Stamenkovic, V. R. Multimetallic Core/Interlayer/Shell Nanostructures as Advanced Electrocatalysts. *Nano Lett.* **2014**, *14*, 6361−6367.

(29) Wang, G.; Huang, B.; Xiao, L.; Ren, Z.; Chen, H.; Wang, D.; Abruña, H. D.; Lu, J.; Zhuang, L. Pt Skin on AuCu Intermetallic Substrate: A Strategy to Maximize Pt Utilization for Fuel Cells. *J. Am. Chem. Soc.* **2014**, *136*, 9643−9649.

(30) Sasaki, K.; Naohara, H.; Choi, Y. M.; Cai, Y.; Chen, W.-F.; Liu, P.; Adzic, R. R. Highly Stable Pt Monolayer on PdAu Nanoparticle Electrocatalysts for the Oxygen Reduction Reaction. *Nat. Commun.* **2012**, *3*, No. 1115.

(31) Sasaki, K.; Naohara, H.; Cai, Y.; Choi, Y. M.; Liu, P.; Vukmirovic, M. B.; Wang, J. X.; Adzic, R. R. Core-Protected Platinum Monolayer Shell High-Stability Electrocatalysts for Fuel-Cell Cathodes. *Angew. Chem., Int. Ed.* **2010**, *49*, 8602−8607.

(32) Dai, Y.; Chen, S. Oxygen Reduction Electrocatalyst of Pt on Au Nanoparticles through Spontaneous Deposition. *ACS Appl. Mater. Interfaces* **2015**, *7*, 823−829.

(33) Kakade, B.; Patil, I.; Lokanathan, M.; Swami, A. Enhanced Methanol Electrooxidation at Pt Skin@PdPt Nanocrystals. *J. Mater. Chem. A* **2015**, *3*, 17771−17779.

(34) Ataee-Esfahani, H.; Wang, L.; Nemoto, Y.; Yamauchi, Y. Synthesis of Bimetallic Au@Pt Nanoparticles with Au Core and Nanostructured Pt Shell toward Highly Active Electrocatalysts. *Chem. Mater.* **2010**, *22*, 6310−6318.

(35) Yu, Y.; Zhang, Q.; Xie, J.; Lee, J. Y. Engineering the Architectural Diversity of Heterogeneous Metallic Nanocrystals. *Nat. Commun.* **2013**, *4*, No. 1454.

(36) Yu, Y.; Zhang, Q.; Yao, Q.; Xie, J.; Lee, J. Y. Architectural Design of Heterogeneous Metallic Nanocrystals-Principles and Processes. *Acc. Chem. Res.* **2014**, *47*, 3530−3540.

(37) Yu, Y.; Zhang, Q.; Yao, Q.; Xie, J.; Lee, J. Y. Guiding Principles in the Galvanic Replacement Reaction of an Underpotentially Deposited Metal Layer for Site-Selective Deposition and Shape and Size Control of Satellite Nanocrystals. *Chem. Mater.* **2013**, *25*, 4746−4756.

(38) Yoon, J.; Baik, H.; Lee, S.; Kwon, S. J.; Lee, K. One-Pot Synthesis of Ultralong Coaxial Au@Pt Nanocables with Numerous Highly Catalytically Active Perpendicular Twinning Boundaries and Au@Pt Core-Shell Bead Structures. *Nanoscale* **2014**, *6*, 6434−6439.

(39) Liu, C.-W.; Wei, Y.-C.; Liu, C.-C.; Wang, K.-W. Pt-Au Core/Shell Nanorods: Preparation and Applications as Electrocatalysts for Fuel Cells. *J. Mater. Chem.* **2012**, *22*, 4641−4644.

(40) Zeng, J.; Yang, J.; Lee, J. Y.; Zhou, W. Preparation of Carbon-Supported Core-Shell Au-Pt Nanoparticles for Methanol Oxidation Reaction: The Promotional Effect of the Au Core. *J. Phys. Chem. B* **2006**, *110*, 24606−24611.

(41) Turkevich, J.; Stevenson, P. C.; Hillier, J. A Study of the Nucleation and Growth Processes in the Synthesis of Colloidal Gold. *Discuss. Faraday Soc.* **1951**, *11*, 55−75.

DOI: 10.1021/acsami.7b08210

(42) Frens, G. Controlled Nucleation for the Regulation of the Particle Size in Monodisperse Gold Suspensions. *Nat. Phys. Sci.* **1973**, *241*, 20−22.

(43) Kresse, G.; Hafner, J. Ab initio Molecular-Dynamics Simulation of the Liquid-Metal-Amorphous-Semiconductor Transition in Germanium. *Phys. Rev. B* **1994**, *49*, 14251−14269.

(44) Kresse, G.; Furthmüller, J. Efficient Iterative Schemes for Ab Initio Total-Energy Calculations Using a Plane-Wave Basis Set. *Phys. Rev. B* **1996**, *54*, 11169−11186.

(45) Blöchl, P. E. Projector Augmented-Wave Method. *Phys. Rev. B* **1994**, *50*, 17953−17979.

(46) Kresse, G.; Joubert, D. From Ultrasoft Pseudopotentials to the Projector Augmented-Wave Method. *Phys. Rev. B* **1999**, *59*, 1758−1775.

(47) Perdew, J. P.; Burke, K.; Ernzerhof, M. Generalized Gradient Approximation Made Simple. *Phys. Rev. Lett.* **1996**, *77*, 3865−3868.

(48) Monkhorst, H. J.; Pack, J. D. Special Points for Brillouin-Zone Integrations. *Phys. Rev. B* **1976**, *13*, 5188−5192.

(49) Lim, B.; Jiang, M.; Camargo, P. H. C.; Cho, E. C.; Tao, J.; Lu, X.; Zhu, Y.; Xia, Y. N. Pd-Pt Bimetallic Nanodendrites with High Activity for Oxygen Reduction. *Science* **2009**, *324*, 1302−1305.

(50) Xie, J.; Lee, J. Y.; Wang, D. I. C. Seedless, Surfactantless, High-Yield Synthesis of Branched Gold Nanocrystals in HEPES Buffer Solution. *Chem. Mater.* **2007**, *19*, 2823−2830.

(51) Xie, J.; Zhang, Q.; Lee, J. Y.; Wang, D. I. C. The Synthesis of SERS-Active Gold Nanoflower Tags for In Vivo Applications. *ACS Nano* **2008**, *2*, 2473−2480.

(52) Bigall, N. C.; Härtling, T.; Klose, M.; Simon, P.; Eng, L. M.; Eychmüller, A. Monodisperse Platinum Nanospheres with Adjustable Diameters from 10 to 100 nm: Synthesis and Distinct Optical Properties. *Nano Lett.* **2008**, *8*, 4588−4592.

(53) Zhao, D.; Xu, B.-Q. Enhancement of Pt Utilization in Electrocatalysts by Using Gold Nanoparticles. *Angew. Chem., Int. Ed.* **2006**, *45*, 4955−4959.